Supplementary Information

Dynamic Covalent Colloidal Gel via RISA for Treating Synergistic Progression of Periodontitis and Dental Demineralization

Haoyue Wu[1,2], Jing Shen[1,*], Fan Yang[1,6], Yuhan Zhao[3], Yi Wu[2], Keqing Jin[1], Yuanfeng Li[3,*], Linqi Shi[2], Yong Liu[2,4,5*]

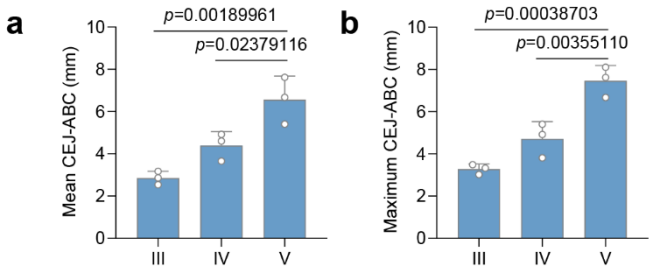

Supplementary Fig. 1 Assessment of alveolar bone loss in subjects with varying degrees of periodontitis. a, b Quantitative analysis of alveolar bone resorption in different subject groups based on panoramic radiographs, showing the mean (**a**) and maximum (**b**) CEJ–ABC distances as indicators of horizontal bone loss.

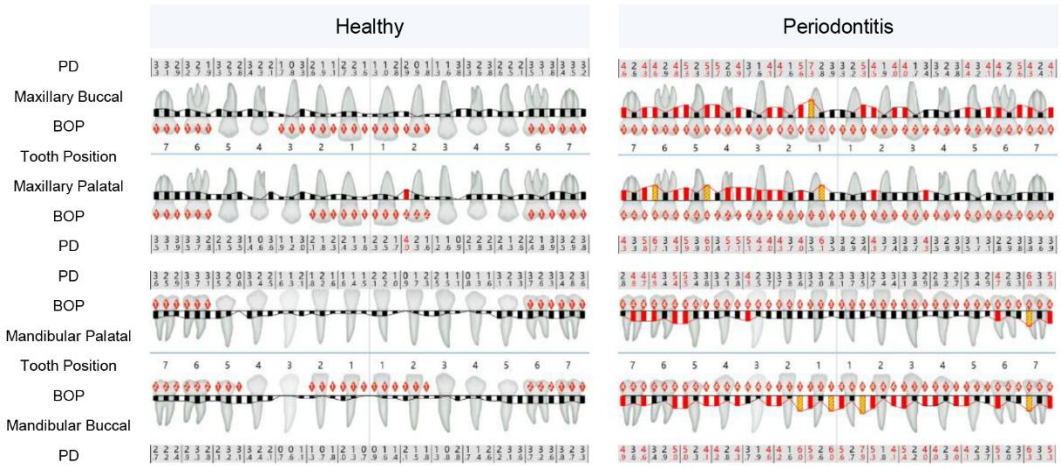

Supplementary Fig. 2 Representative full-mouth scans acquired by electronic periodontal probing in healthy and periodontitis subjects.

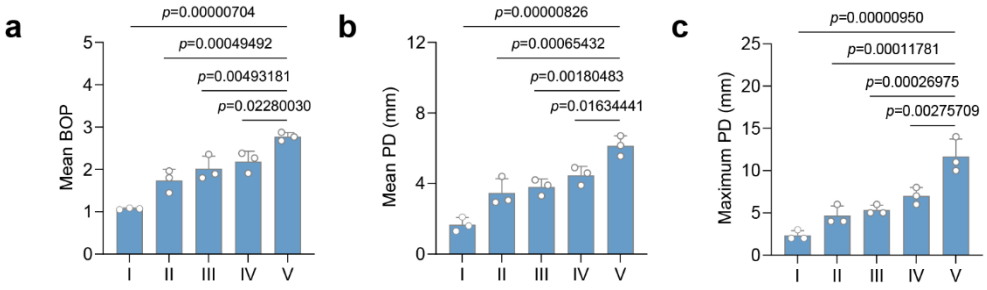

Supplementary Fig. 3 Quantitative analysis of periodontal bleeding and pocket depth in subjects with different periodontal statuses. a–c Quantitative assessment based on electronic periodontal probe scans showing the mean BOP (**a**), mean PD (**b**), and maximum PD (**c**) in each subject group.

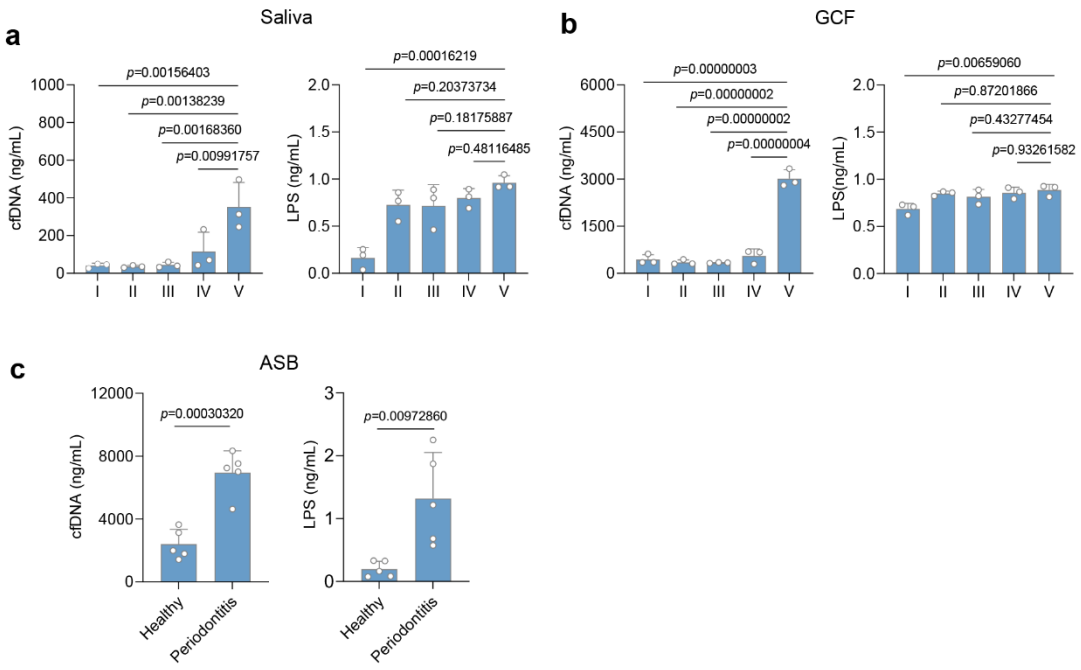

Supplementary Fig. 4 Analysis of cfDNA and LPS levels in body fluid samples from subjects with different periodontal conditions. a–c Quantification of cfDNA and LPS in saliva (**a**), GCF (**b**), and ASB (**c**) from different subject groups, to evaluate the distribution of inflammation-related PAMPs and DAMPs across multiple biological fluids.

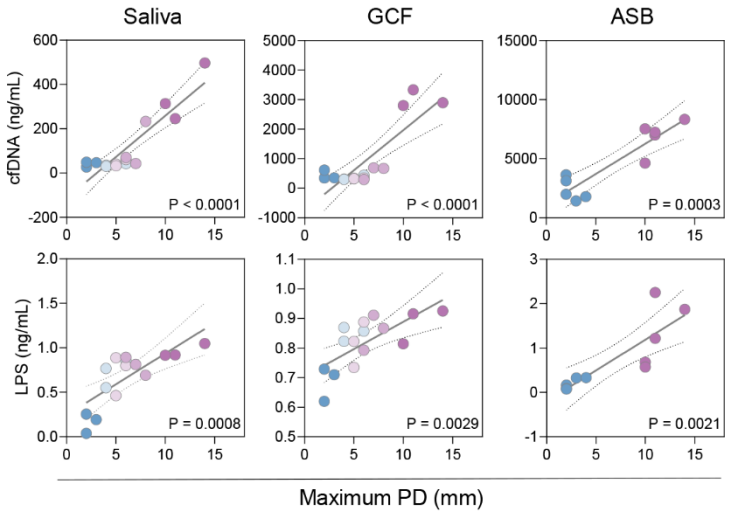

Supplementary Fig. 5 Scatter plots showing the correlation between cfDNA and LPS levels in saliva, GCF, and ASB and the maximum PD.

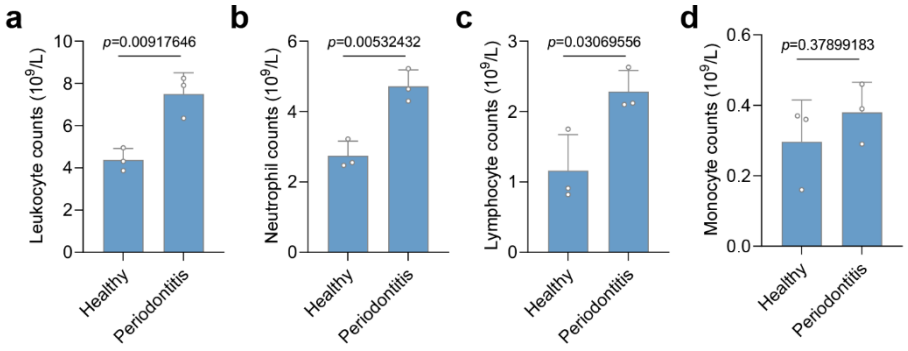

Supplementary Fig. 6 Analysis of inflammatory cell counts in PVB of different subject groups. a–d Quantitative comparison of total leukocytes (**a**), neutrophils (**b**), lymphocytes (**c**), and monocytes (**d**) in peripheral blood samples from healthy subjects and periodontitis patients.

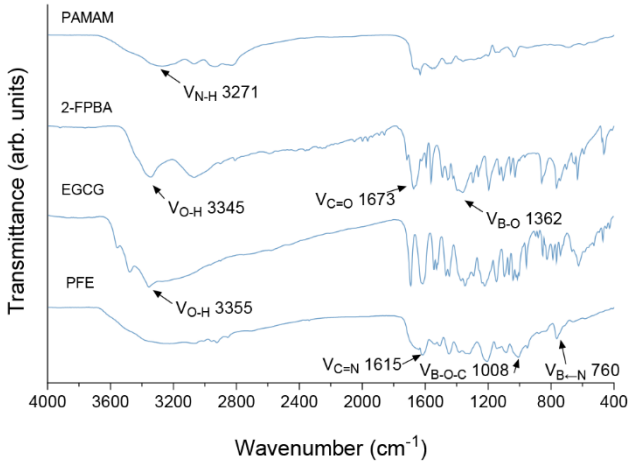

Supplementary Fig. 7 FT-IR spectra of PAMAM, 2-FPBA, EGCG, and PFE.

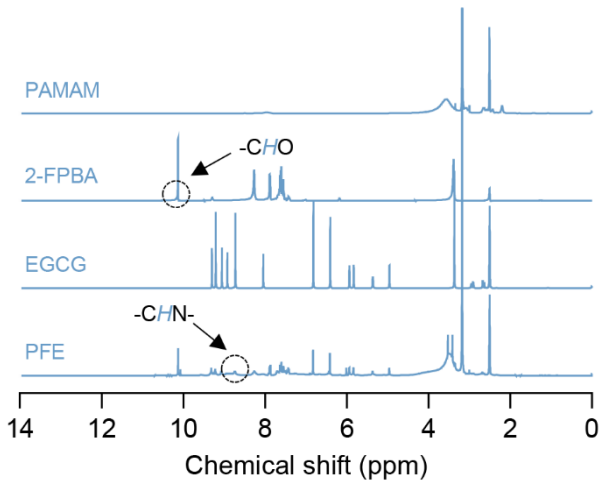

Supplementary Fig. 8 ^{1}H NMR spectra of PAMAM, EGCG, 2-FPBA, and PFE measured in DMSO-d_6 solvent.

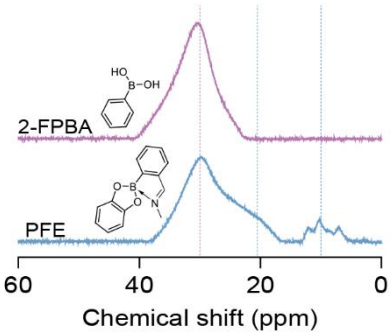

Supplementary Fig. 9 ^{11}B NMR spectra of 2-FPBA and PFE measured in DMSO-d_6 solvent.

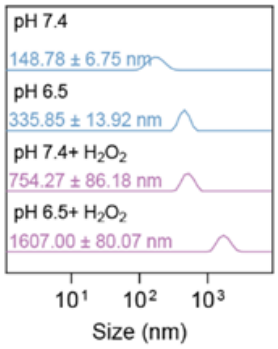

Supplementary Fig. 10 Particle size changes of PFE nanoparticles under acidic and ROS-rich conditions.

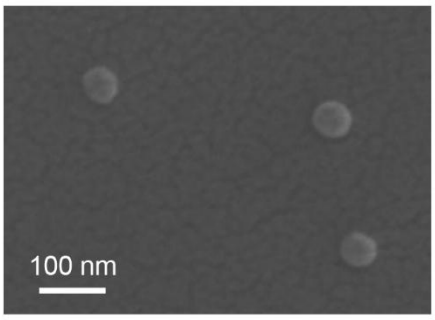

Supplementary Fig. 11 Representative SEM images of PFE nanoparticles.

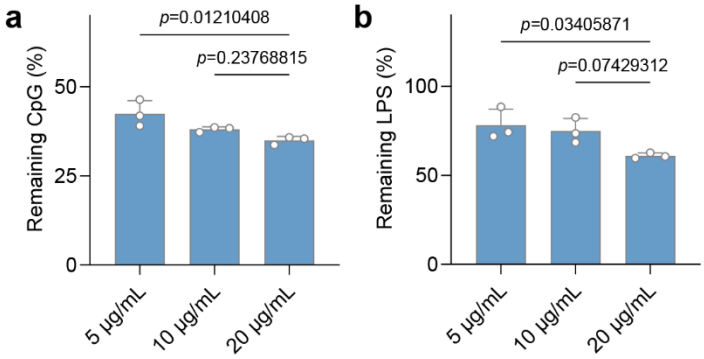

Supplementary Fig. 12 Assessment of the adsorption capacity of PFE CGs toward CpG and LPS at varying concentrations. a, b Adsorption efficiency of PFE CGs toward CpG (**a**) and LPS (**b**) at different concentrations. The concentration-dependent adsorption was evaluated by quantifying the residual amounts of unbound CpG and LPS.

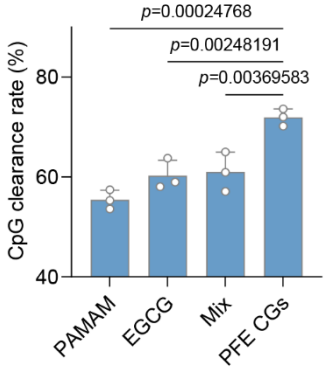

Supplementary Fig. 13 Evaluation of CpG clearance capacity of different materials at the cellular level.

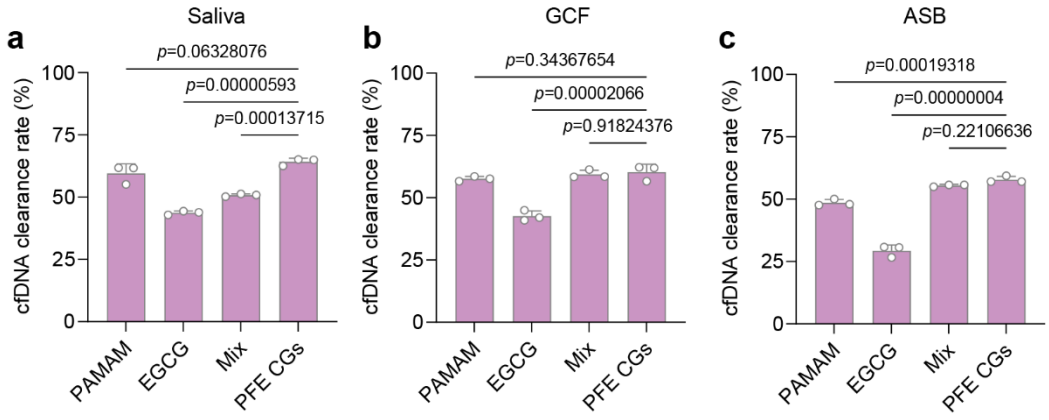

Supplementary Fig. 14 Evaluation of cfDNA clearance capacity of different materials in clinical fluid samples. a–c Saliva (**a**), GCF (**b**), and ASB (**c**) samples collected from clinical subjects were treated with PAMAM, EGCG, Mix, or PFE CGs. Residual cfDNA levels were quantified to assess the clearance efficiency of each material across different biological fluids.

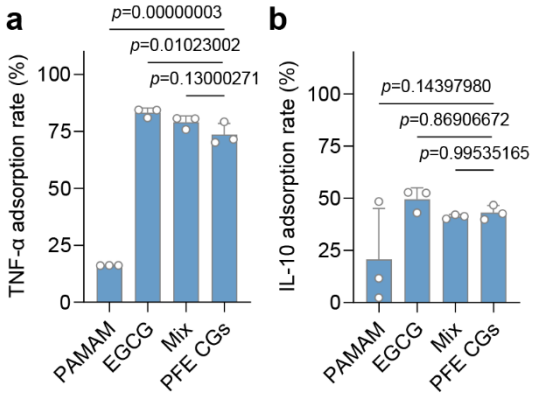

Supplementary Fig. 15 Evaluation of the adsorption capacity of different materials for inflammation-related cytokines *in vitro*. a, b The adsorption rates of PAMAM, EGCG, Mix, and PFE CGs toward the pro-inflammatory cytokine TNF-α (**a**) and the anti-inflammatory cytokine IL-10 (**b**) were measured to quantitatively assess the selective adsorption properties of each material for inflammation-associated cytokines.

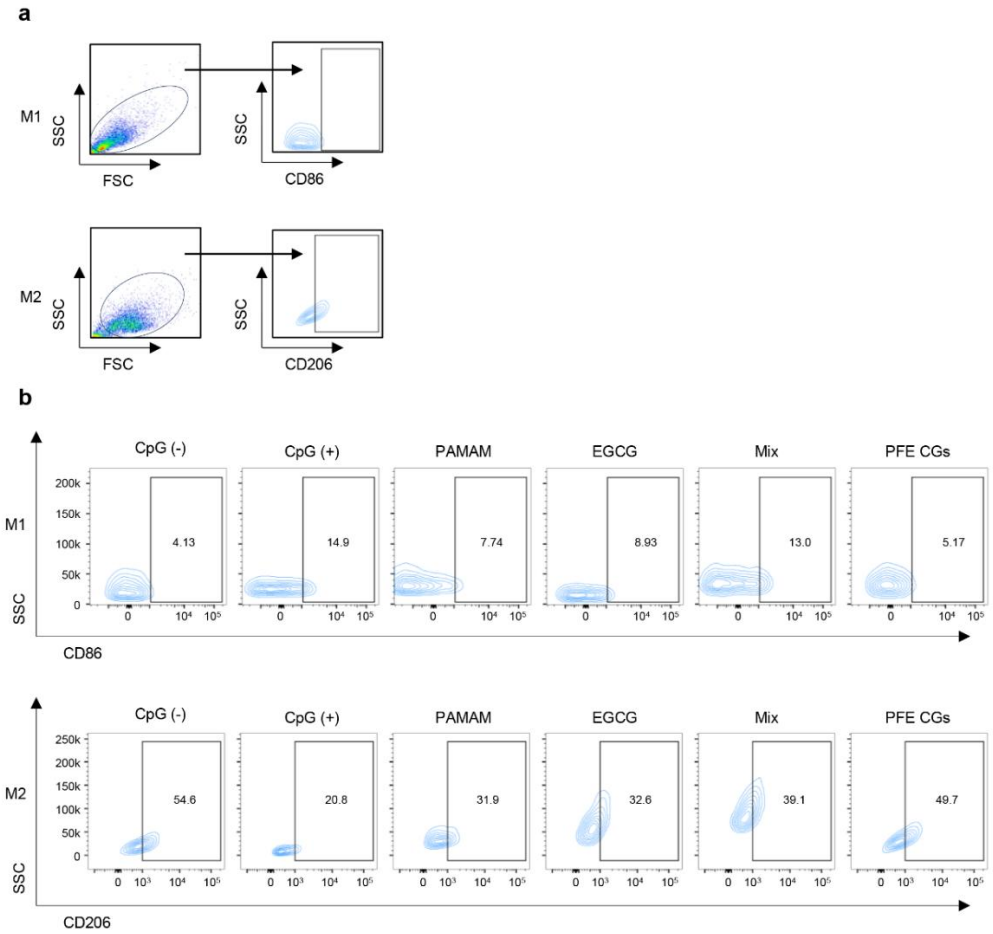

Supplementary Fig. 16 Effects of different treatments on CpG-induced macrophage polarization. a Gating strategy to identify M1 and M2 macrophage. **b** Representative flow cytometry images.

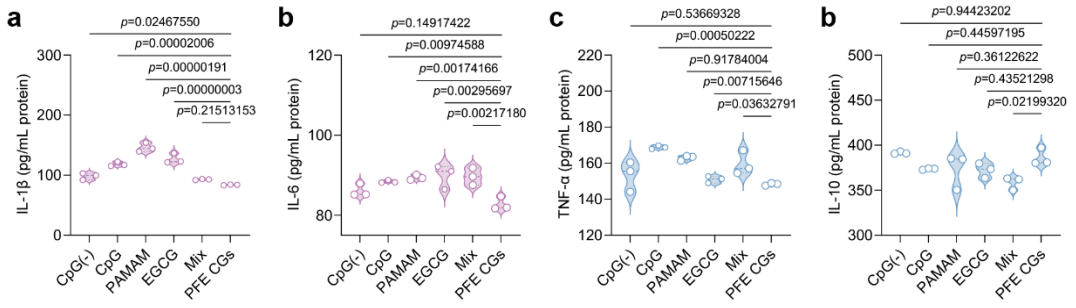

Supplementary Fig. 17 ELISA detection of inflammatory cytokines. a-d ELISA results showing the levels of inflammatory cytokines IL-1β (**a**), IL-6 (**b**), TNF-α (**c**), and anti-inflammatory cytokine IL-10 (**d**) in the supernatants of CpG-stimulated RAW 264.7 macrophages treated with various materials for 12 hours.

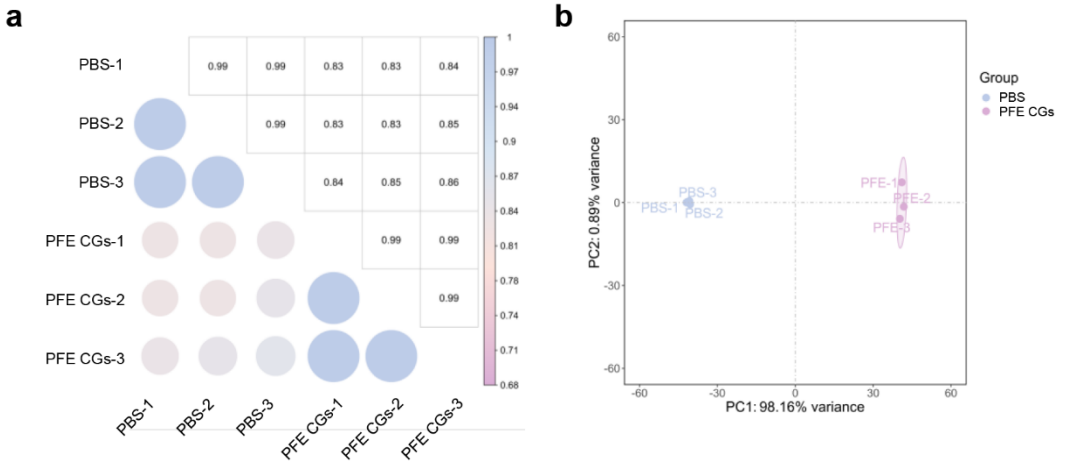

Supplementary Fig. 18 Quality assessment of transcriptome sequencing samples. a Correlation analysis of inter-sample expression data to evaluate consistency and reproducibility among sequencing samples. **b** PCA for dimensionality reduction, illustrating the clustering patterns of samples across different groups.

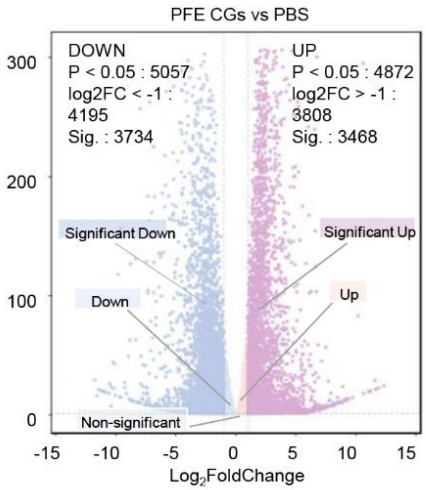

Supplementary Fig. 19 Volcano plot showing the distribution of DEGs between the PFE CGs and PBS groups. Genes significantly upregulated in the PFE CGs treatment group compared to the PBS control are indicated on the right, while significantly downregulated genes are shown on the left.

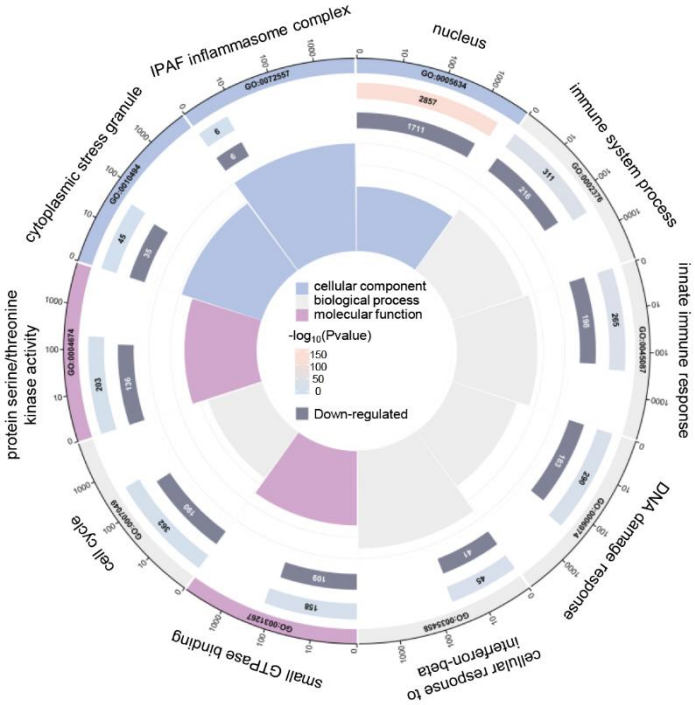

Supplementary Fig. 20 Circular bar plots displaying GO enrichment analysis of downregulated genes in the PFE CGs-treated group compared to the PBS-treated group.

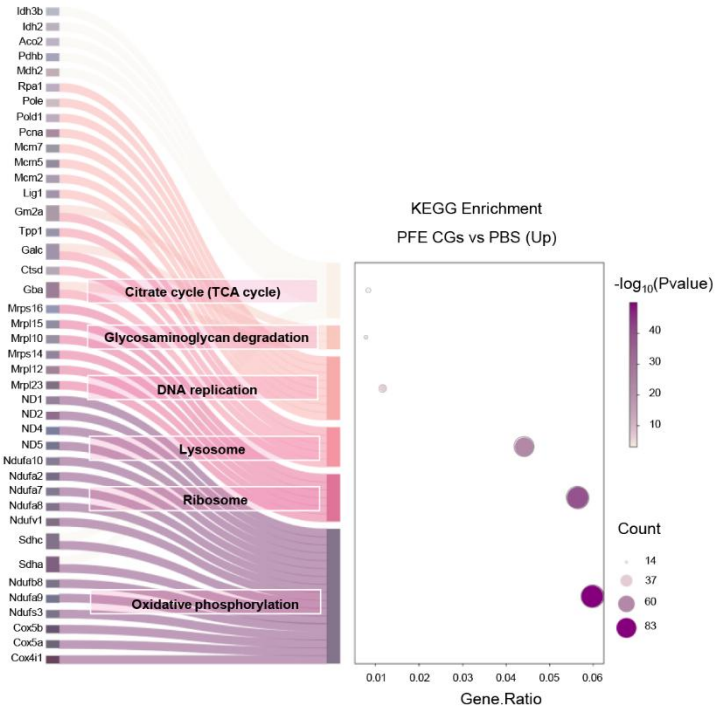

Supplementary Fig. 21 Sankey bubble plots illustrating KEGG pathway enrichment of upregulated genes.

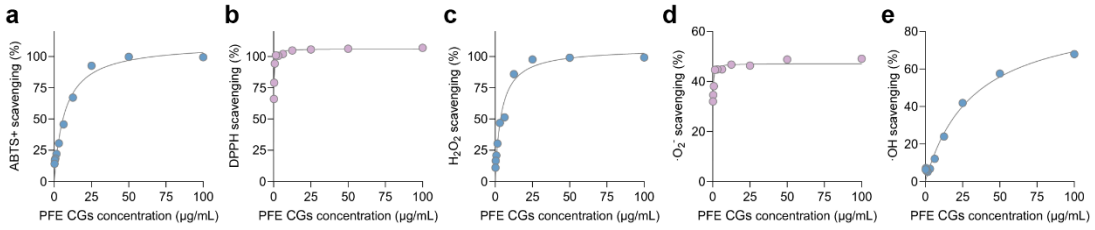

Supplementary Fig. 22 Detection of free radical scavenging capacity. a-e Scavenging efficiencies of PFE CGs against $ABTS^+$ (**a**), DPPH (**b**), H_2O_2 (**c**), $\bullet O_2^-$ (**d**), and •OH (**e**) at various concentrations.

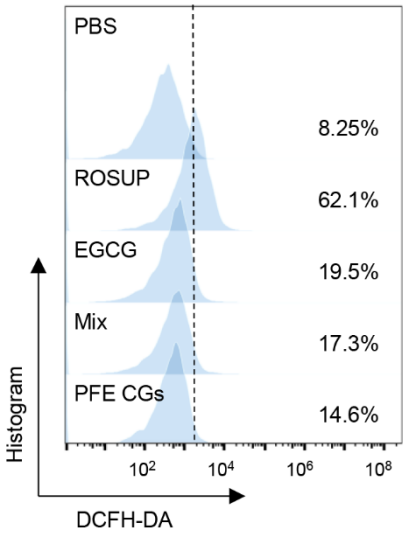

Supplementary Fig. 23 Intracellular ROS levels in RAW 264.7 macrophages treated with PFE CGs or control materials following ROSUP stimulation, assessed by flow cytometry.

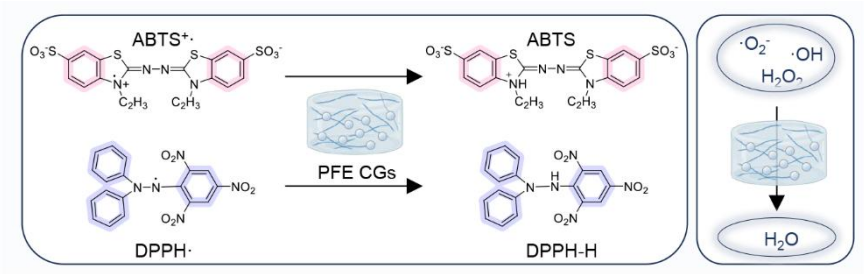

Supplementary Fig. 24 Schematic illustration summarizing the broad-spectrum ROS-scavenging capability of PFE CGs.

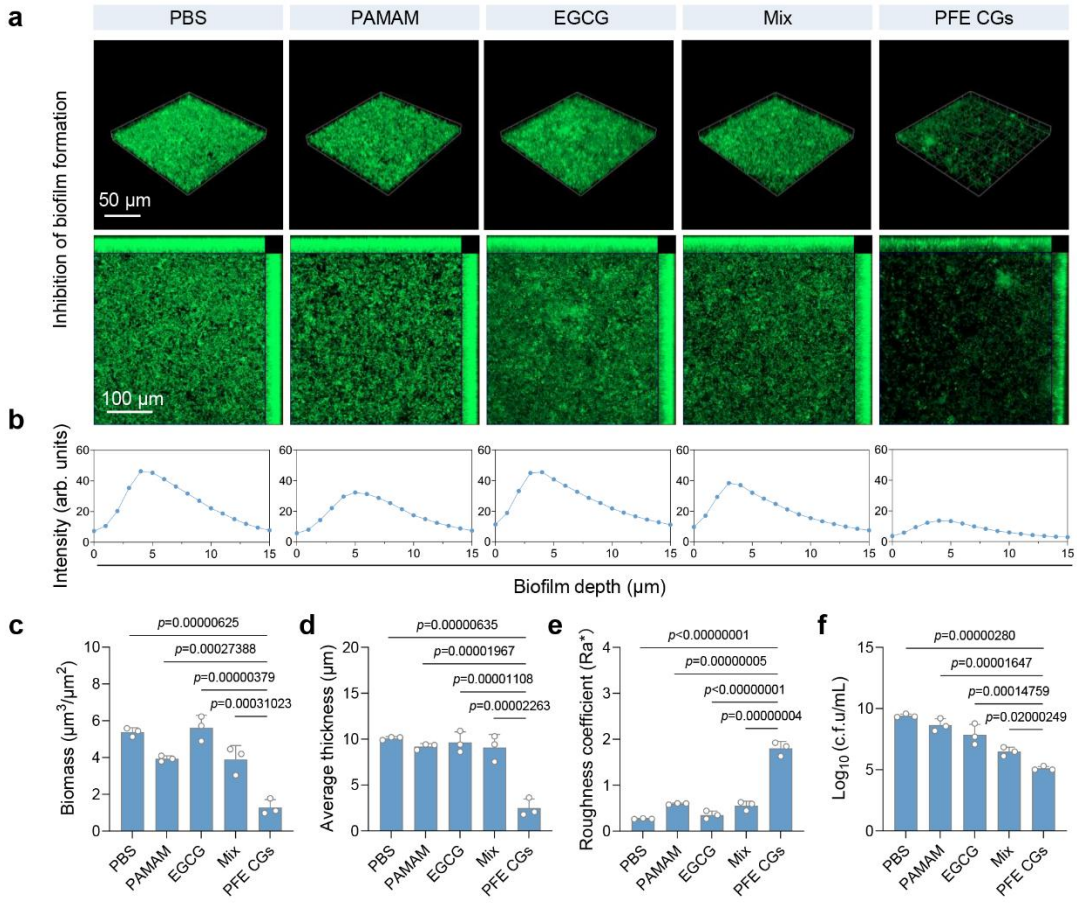

Supplementary Fig. 25 Inhibitory effects of PFE CGs on *P. gingivalis* biofilms. a Representative 3D and planar fluorescence images of live *P. gingivalis* in biofilms following different treatments, captured by CLSM. **b** Quantitative analysis of the distribution of green fluorescence intensity relative to biofilm depth based on CLSM images. **c–e** Quantification of biofilm biomass (**c**), average thickness (**d**), and roughness (**e**) of *P. gingivalis* biofilms using ImageJ software equipped with the COMSTAT plugin (n = 3). **f** Bacterial viability within *P. gingivalis* biofilms from different treatment groups assessed by CFU counting.

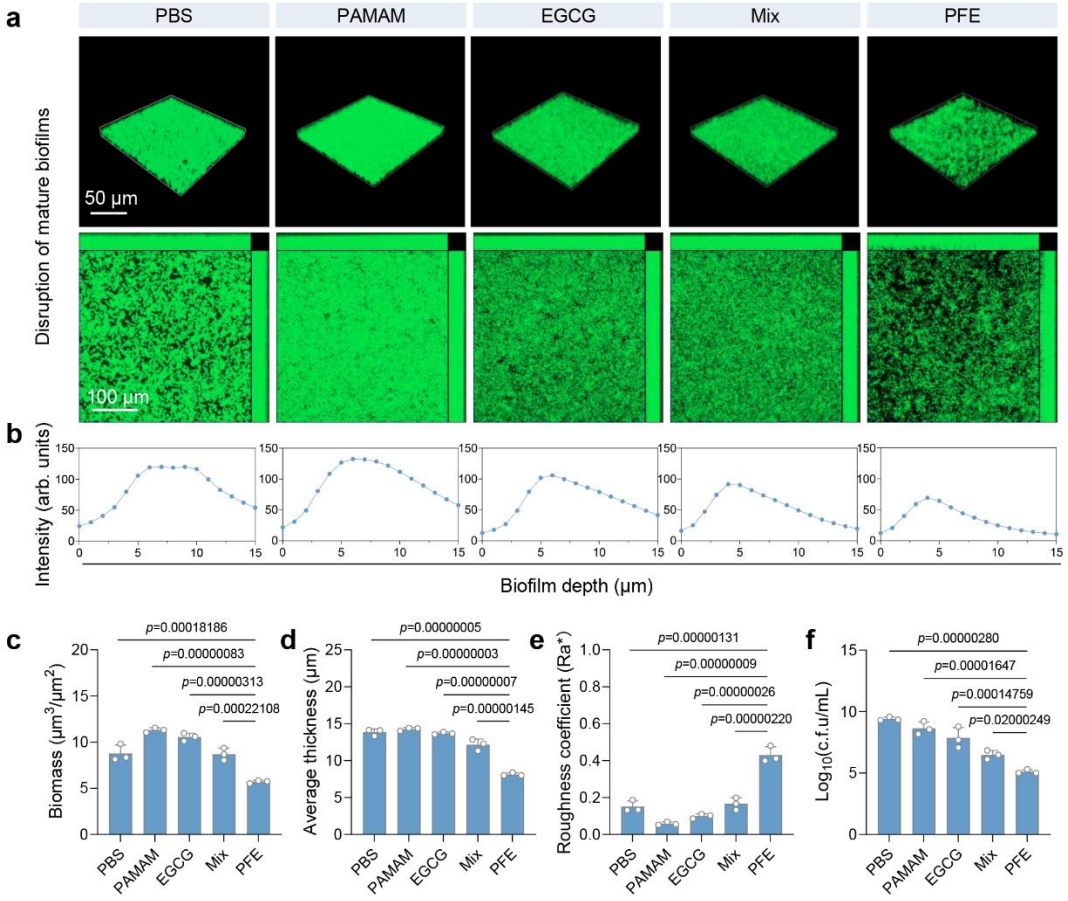

Supplementary Fig. 26 Disruption of mature *P. gingivalis* biofilms by PFE CGs. a Representative 3D and planar fluorescence images of live *P. gingivalis* in biofilms following different treatments, captured by CLSM. **b** Quantitative analysis of the distribution of green fluorescence intensity relative to biofilm depth based on CLSM images. **c–e** Quantification of biofilm biomass (**c**), average thickness (**d**), and roughness (**e**) of *P. gingivalis* biofilms using ImageJ software equipped with the COMSTAT plugin (*n* = 3). **f** Bacterial viability within *P. gingivalis* biofilms from different treatment groups assessed by CFU counting.

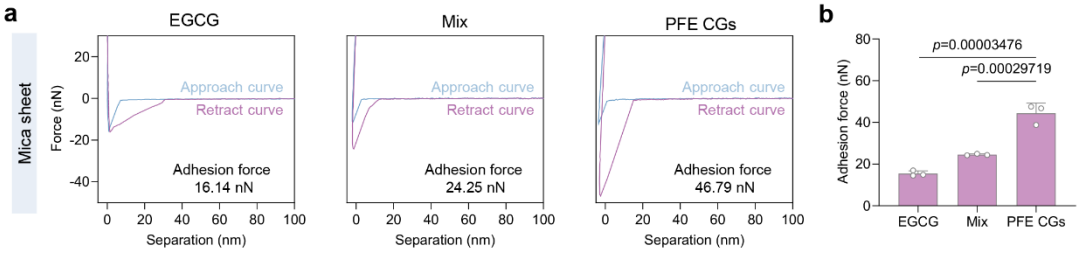

Supplementary Fig. 27 Material adhesion on mica surfaces. a AFM measurements of approach and retract force curves of EGCG, Mix, and PFE CGs on mica surfaces to evaluate single-point adhesion force. **b** Quantitative analysis of multiple-point adhesion forces of different materials on mica surfaces.

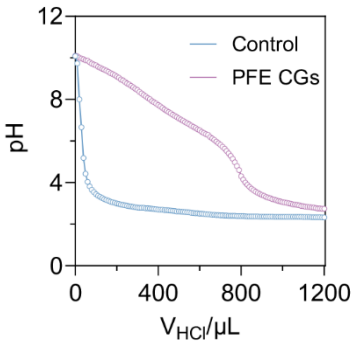

Supplementary Fig. 28 Titration curve of hydrochloric acid demonstrating the pH buffering capacity of PFE CGs.

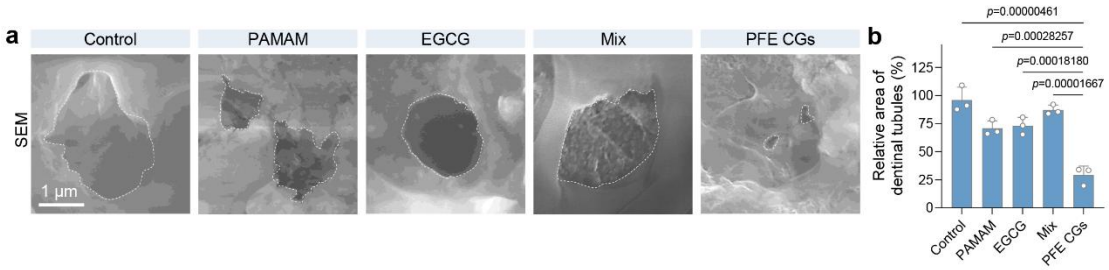

Supplementary Fig. 29 Evaluation of dentinal tubule occlusion following treatment with different materials. a Representative SEM images showing dentinal tubule occlusion in each treatment group. **b** Quantitative analysis of dentinal tubule exposure area from SEM images.

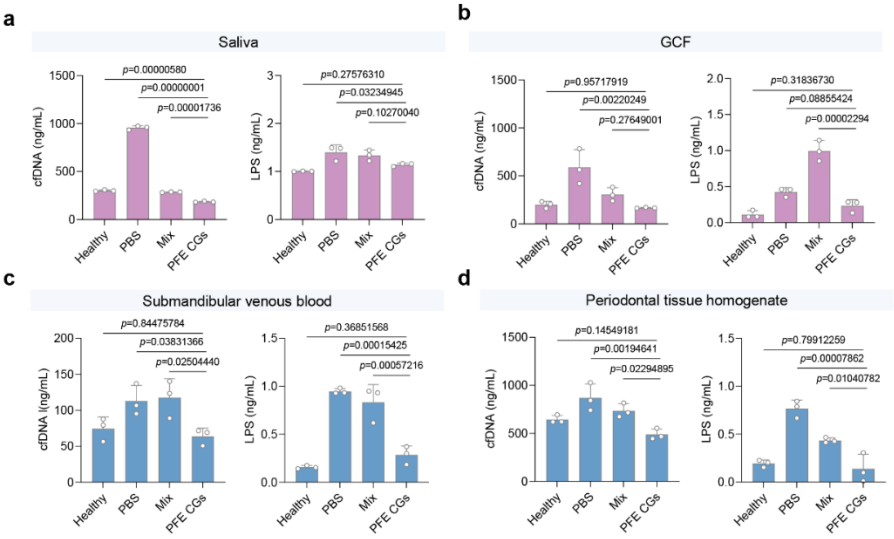

Supplementary Fig. 30 Quantitative analysis of inflammation-related molecules in rats following different treatments. a–d Measurement of cfDNA and LPS concentration in rat saliva (**a**), GCF (**b**), submandibular venous blood (**c**), and periodontal tissue homogenates (**d**).

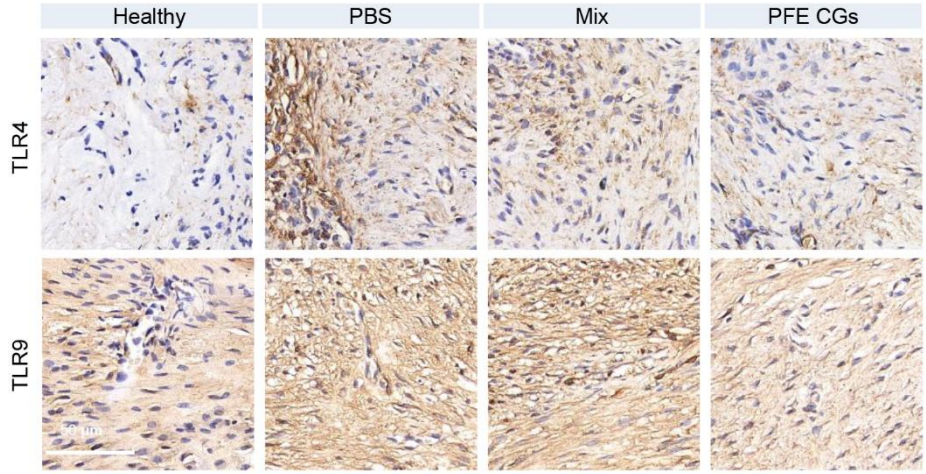

Supplementary Fig. 31 Representative IHC images comparing TLR4 and TLR9 expression levels in periodontal tissues across different groups.

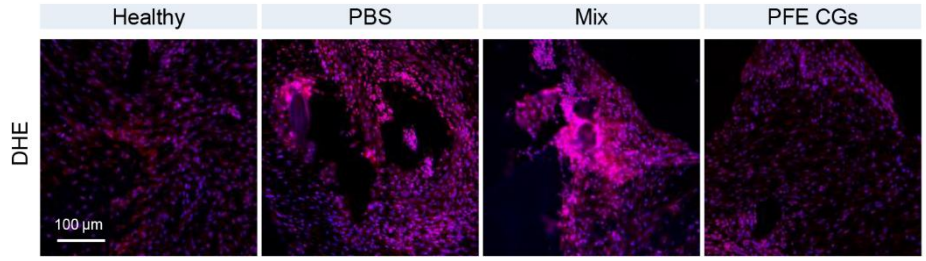

Supplementary Fig. 32 DHE fluorescence staining of periodontal tissues from different treatment groups in rats.

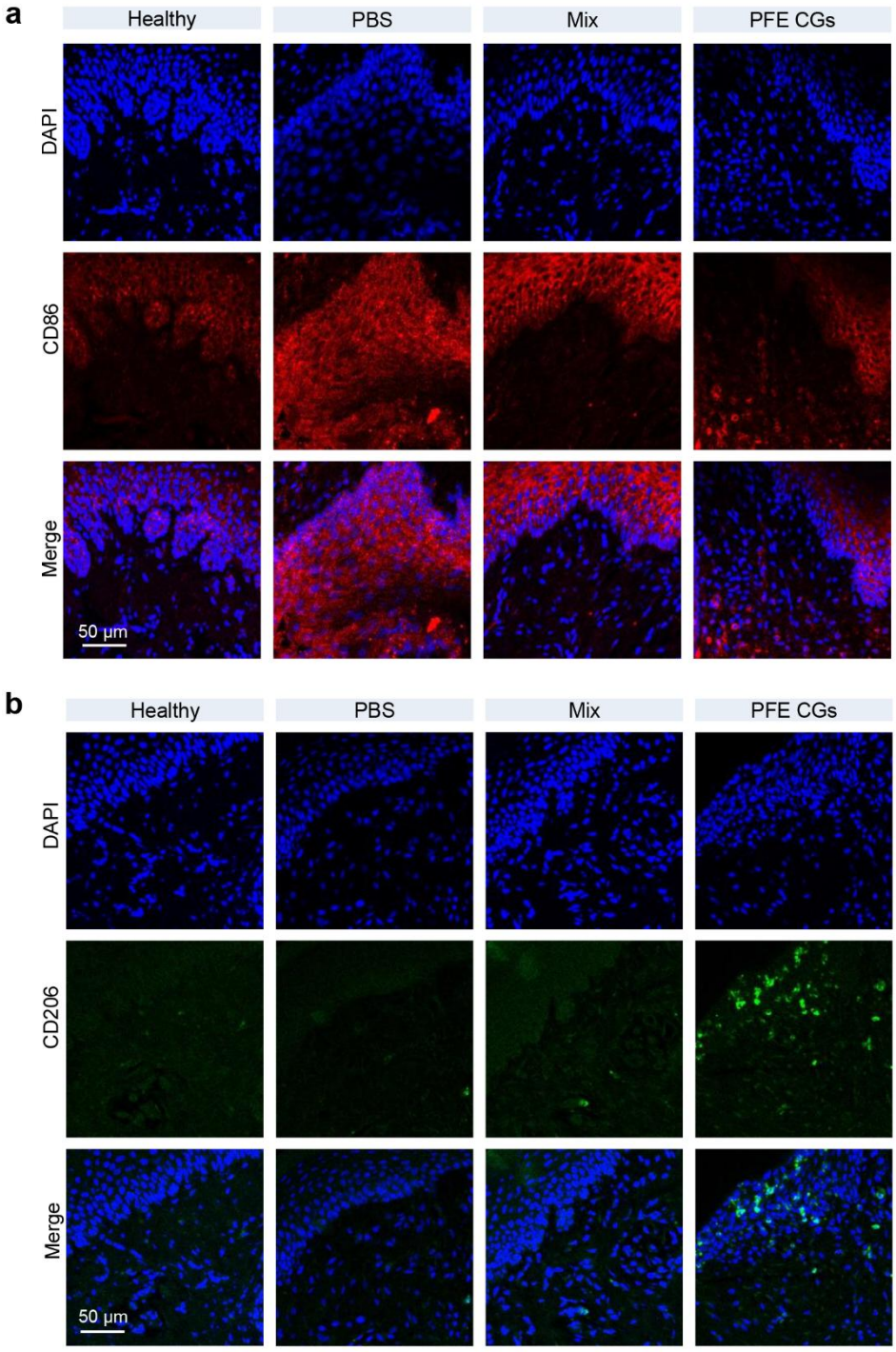

Supplementary Fig. 33 Immunofluorescence analysis of macrophage polarization markers in periodontal tissues from rats subjected to different treatments. a Representative fluorescence images of the M1 macrophage marker CD86 in periodontal tissues across groups. **b** Representative fluorescence images of the M2 macrophage marker CD206 in periodontal tissues across groups.

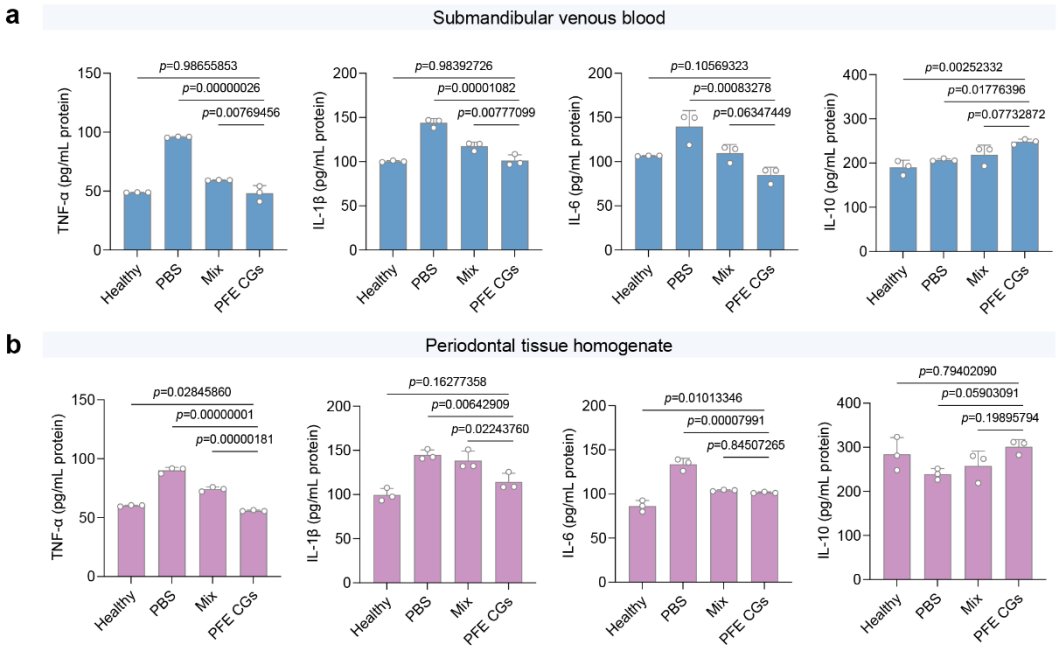

Supplementary Fig. 34 ELISA analysis of inflammatory cytokine levels in submandibular venous blood and periodontal tissues of rats following different treatments. **a** Concentrations of TNF-α, IL-1β, IL-6, and IL-10 measured in submandibular venous blood. **b** Concentrations of the same cytokines measured in periodontal tissue homogenates. Data are presented as mean ± SD from n = 3 biologically independent rats.

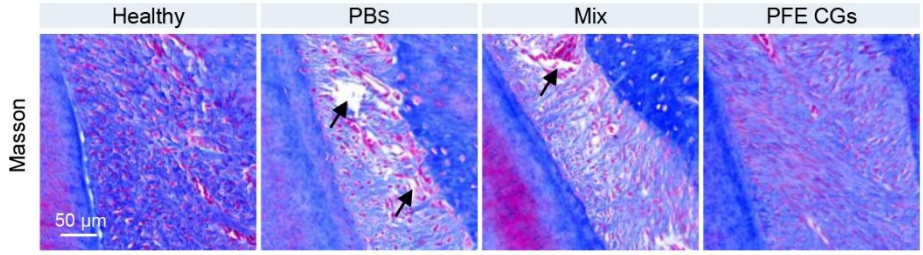

Supplementary Fig. 35 Representative Masson's trichrome staining images of periodontal tissues from rats in different treatment groups.

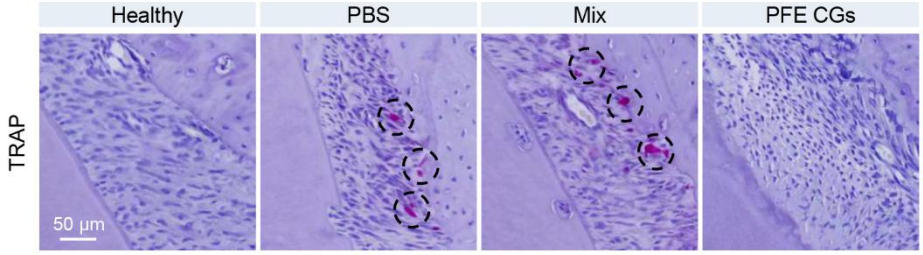

Supplementary Fig. 36 Representative TRAP staining images of periodontal tissues from rats in different treatment groups.

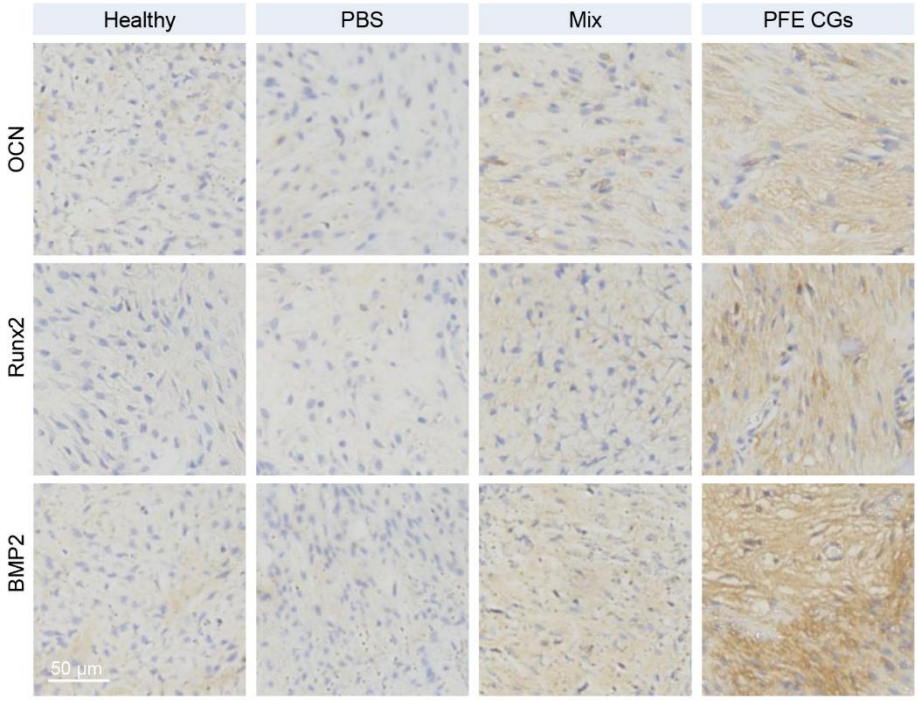

Supplementary Fig. 37 Representative IHC images comparing the expression levels of OCN, Runx2, and BMP2 in periodontal tissues across different groups.

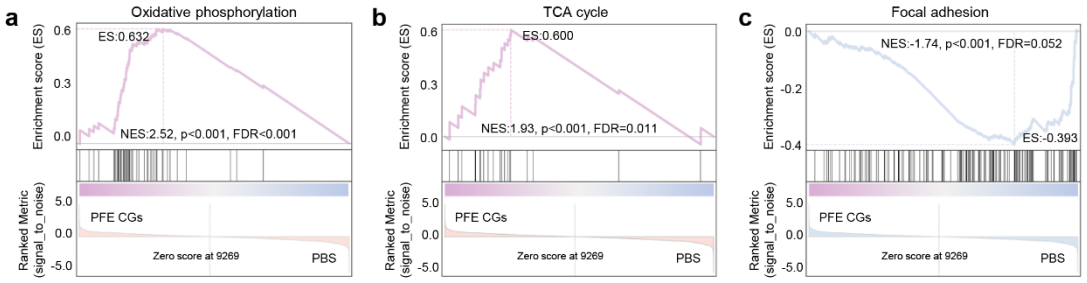

Supplementary Fig. 38 GSEA reveals significant alterations in pathways associated with DEGs. a-c Compared to the PBS group, the PFE CGs treatment group shows significant enrichment or suppression in key signaling pathways, including oxidative phosphorylation (**a**), the TCA cycle (**b**), and focal adhesion (**c**).

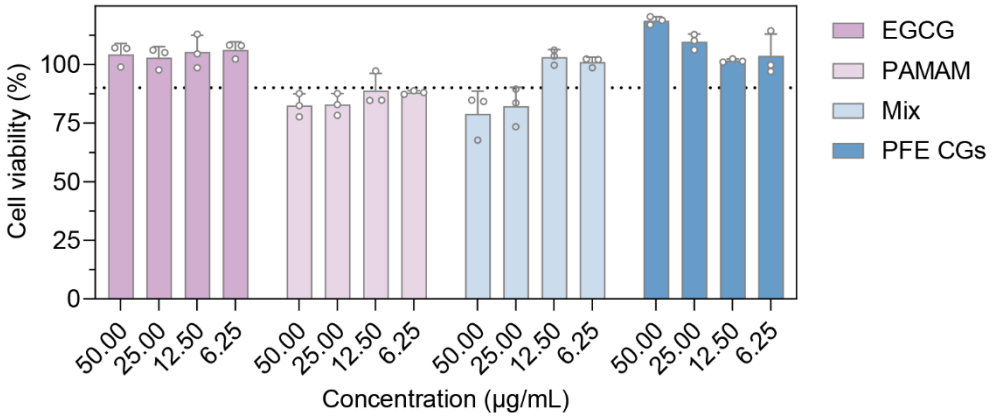

Supplementary Fig. 39 Cell viability of 3T3 fibroblasts following treatment with different concentrations of PAMAM, EGCG, Mix, and PFE CGs.

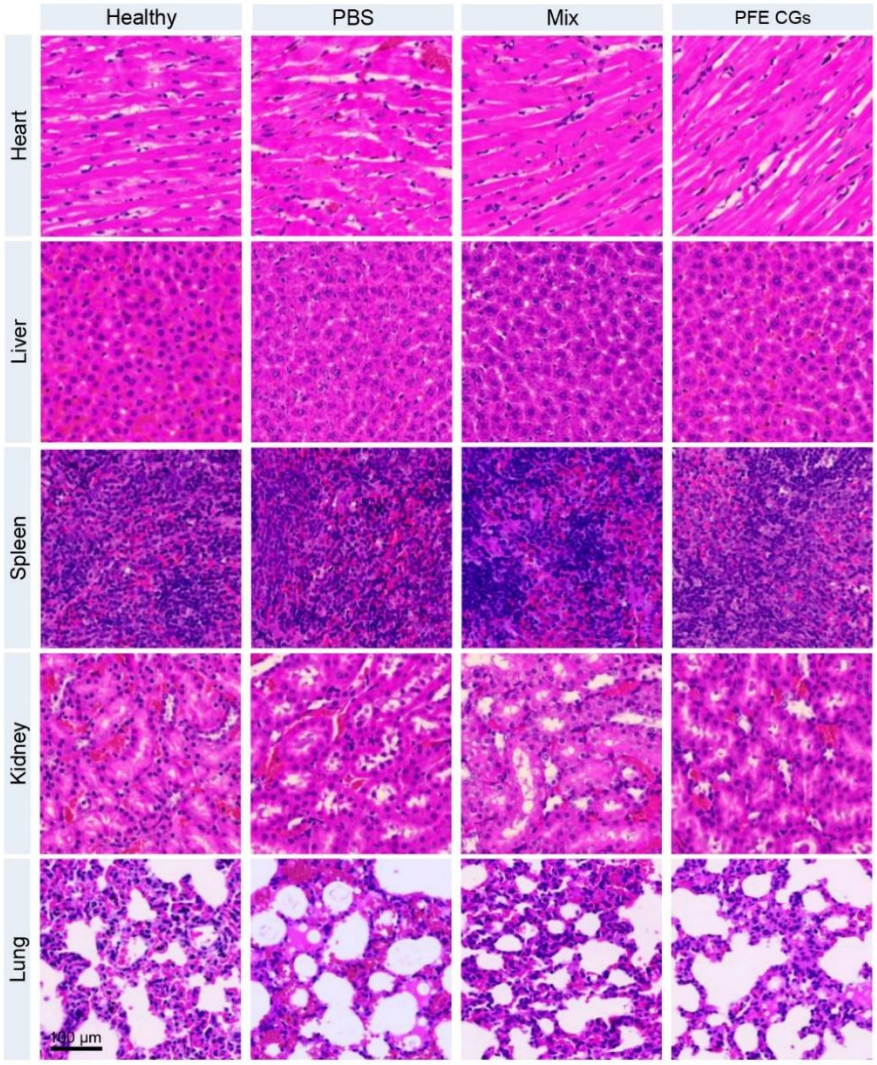

Supplementary Fig. 40 Representative H&E staining images of major organs from rats in different treatment groups.

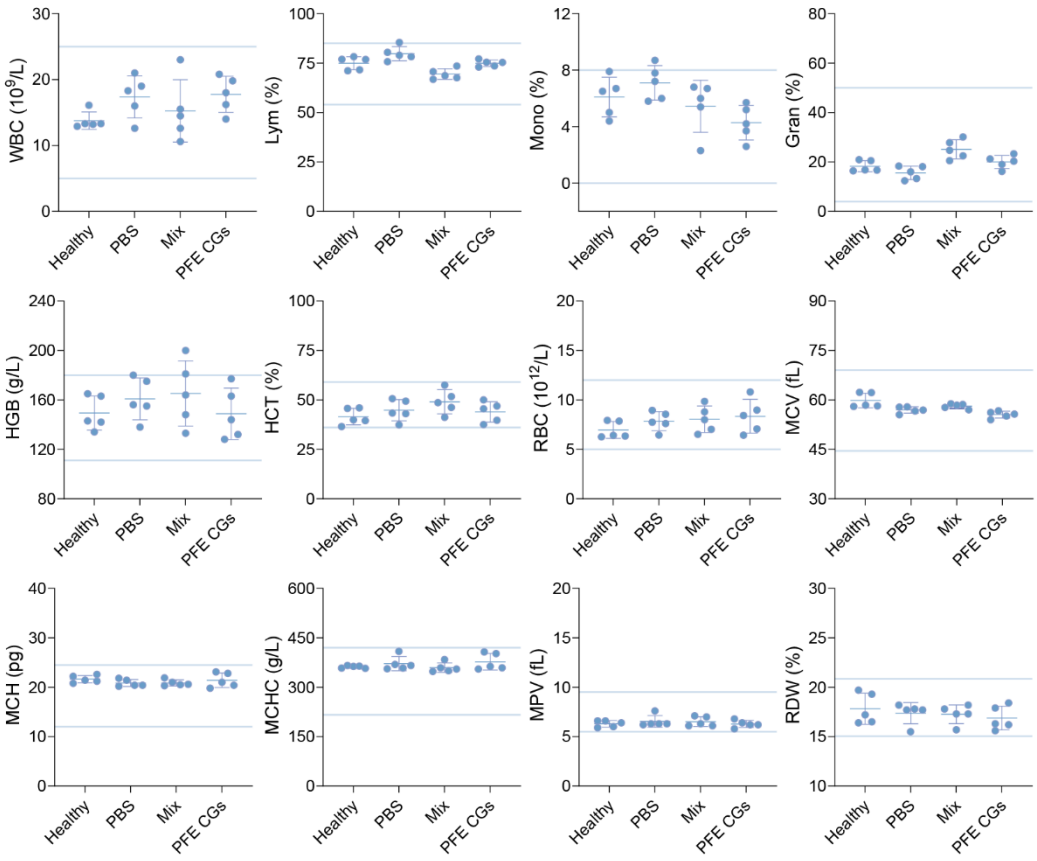

Supplementary Fig. 41 Quantitative analysis of hematological parameters in peripheral blood from rats across different treatment groups. Multiple blood indices were statistically analyzed, including white blood cell count (WBC), lymphocyte count (Lym), monocyte count (Mono), granulocyte count (Gran), hemoglobin concentration (HGB), hematocrit (HCT), red blood cell count (RBC), mean corpuscular volume (MCV), mean corpuscular hemoglobin (MCH), mean corpuscular hemoglobin concentration (MCHC), mean platelet volume (MPV), and red cell distribution width (RDW).

Supplementary Table 1. Component ratios used in the preparation of 1 mL PFE CGs.

	n (μmol)	Molecular weight	m (mg)
PAMAM-G3	8.70	6908.83	0.20
2-FPBA	13.92	149.94	0.70
EGCG	6.96	458.37	1.06

Supplementary Table 2 List of primer sequences used for qPCR analysis.

ID	Reference Sequence	Gene Name	Forward primer (3'-5')	Reverse primer (5'-3')	Size
81897	NM_031178.2	TLR9	TCTCACGCCTCCAGTGTCTTAGC	GCAGATTAGTCAGCGGCAGGAAC	87
21898	NM_021297.3	TLR4	AAGGCATGGCATGGCTTACACC	GTCTCCACAGCCACCAGATTCTC	122
17874	NM_010851.3	MyD88	AGCAGAACCAGGAGTCCGAGAAG	GGTGATGCCTCCCAGTTCCTTTG	86
18033	NM_001410442.1	NF-kB	TCTACAAGCAGAAGGCGGAGGAG	AGTGCTGTCAGGGAGGAAGGC	142
18035	NM_010907.2	IκBα	ATCACCAACCAGCCAGGAATTGC	CTGCGTCAAGACTGCTACACTGG	138
21926	NM_001278601.1	TNF-α	GCCACCACGCTCTTCTGTCTAC	GGTTTGTGAGTGTGAGGGTCTGG	118
16176	NM_008361.4	IL-1β	TCGCAGCAGCACATCAACAAGAG	AGGTCCACGGGAAAGACACAGG	97
16193	NM_001314054.1	IL-6	GCCTTCTTGGGACTGATGCT	GACAGGTCTGTTGGGAGTGG	99
18126	NM_001313921.1	NOS_2	GCAGGGAATCTTGGAGCGAGTTG	TAGGTGAGGGCTTGGCTGAGTG	138
16153	NM_010548.2	IL-10	TCCCTGGGTGAGAAGCTGAAGAC	CACCTGCTCCACTGCCTTGC	96
14433	NM_001289726.2	GAPDH	AAGGTCGGTGTGAACGGATTTG	ACAATCTCCACTTTGCCACTGC	80

Supplementary Table 3 EDS elemental mapping analysis showing the weight percentages (Wt%) and atomic percentages (At%) of C, O, Ca, and P on the tooth surface across different treatment groups.

	PBS		PAMAM		EGCG		Mix		PFE CGs	
	Wt%	At%	Wt%	At%	Wt%	At%	Wt%	At%	Wt%	At%
C	47.3	59.3	41.5	49.2	42.0	53.5	61.0	71.2	37.5	52.3
O	35.5	33.4	37.1	41.3	40.8	33.4	27.7	24.3	32.3	33.8
Ca	10.1	3.8	12.9	5.1	10.0	3.8	6.4	2.3	19.1	8.0
P	7.2	3.5	8.6	4.4	7.2	3.5	4.9	2.2	11.0	6.0

Supplementary Movie 1 Movie demonstrating the formation process of PFE during preparation.

Supplementary Movie 2 Movie demonstrating the formation process of Mix under the same conditions.